CENTURY-SCALE CHANGE IN WATER AVAILABILITY: CO_2-QUADRUPLING EXPERIMENT

S. MANABE [1], R. T. WETHERALD [2], P. C. D. MILLY [3], T. L. DELWORTH [2] and R. J. STOUFFER [2]

[1] *Program in Atmospheric and Oceanic Sciences, P.O. Box CN710, Sayre Hall, Forrestal Campus, Princeton University, Princeton, NJ 08544-0710, U.S.A.*
E-mail: manabe@splash.princeton.edu
[2] *Geophysical Fluid Dynamics Laboratory/NOAA, P.O. Box 308, Princeton University, Princeton, NJ 08542, U.S.A.*
[3] *U.S. Geological Survey, GFDL/NOAA, P.O. Box 308, Princeton, NJ 08542, U.S.A.*

Abstract. It has been suggested that, unless a major effort is made, the atmospheric concentration of carbon dioxide may rise above four times the pre-industrial level in a few centuries. Here we use a coupled atmosphere-ocean-land model to explore the response of the global water cycle to such a large increase in carbon dioxide, focusing on river discharge and soil moisture. Our results suggest that water is going to be more plentiful in those regions of the world that are already 'water-rich'. However, water stresses will increase significantly in regions and seasons that are already relatively dry. This could pose a very challenging problem for water-resource management around the world. For soil moisture, our results indicate reductions during much of the year in many semi-arid regions of the world, such as the southwestern region of North America, the northeastern region of China, the Mediterranean coast of Europe, and the grasslands of Australia and Africa. In some of these regions, soil moisture values are reduced by almost a factor of two during the dry season. The drying in semi-arid regions is likely to induce the outward expansion of deserts to the surrounding regions. Over extensive regions of both the Eurasian and North American continents in high and middle latitudes, soil moisture decreases in summer but increases in winter, in contrast to the situation in semi-arid regions. For river discharge, our results indicate an average increase of ∼15% during the next few centuries. The discharges from Arctic rivers such as the Mackenzie and Ob' increase by much larger fractions. In the tropics, the discharges from the Amazonas and Ganga-Brahmaputra also increase considerably. However, the percentage changes in runoff from other tropical and many mid-latitude rivers are smaller.

1. Introduction

The study of Walker and Kasting (1992) shows that draconian measures would probably be required to prevent the atmospheric CO_2 concentration from quadrupling in a few centuries. Using a coupled atmosphere-ocean-land model developed at the Geophysical Fluid Dynamics Laboratory of NOAA, this study explores the century-scale change in water availability (i.e., river discharge and soil moisture) that could occur in response to the quadrupling of the CO_2 concentration of the atmosphere.

Climatic Change **64:** 59–76, 2004.

The century-scale response of climate to the quadrupling of atmospheric carbon dioxide was the subject of an earlier study (Manabe and Stouffer, 1993, 1994). However, the simulated distribution of precipitation was not realistic enough for the study of the CO_2-induced change in water availability. Owing to the simplicity of the model and the availability of a powerful computer, it has become feasible to conduct many long term integrations of a coupled model with twice the resolution of the previous model. The simulated, large-scale distribution of precipitation thus obtained (Delworth et al., 2002) is sufficiently realistic for the study conducted here. Encouraged by the improved performance of the coupled model with higher resolution, Wetherald and Manabe (2002) conducted a multi-member ensemble of numerical experiments, and investigated the change in water availability which is expected to occur by the middle of the 21st century under the IS92a scenario (IPCC, 1992). The present study describes and discusses the much larger and more distinct multi-century changes in simulated soil moisture and runoff that result from a quadrupling of atmospheric carbon dioxide.

2. Coupled Atmosphere-Ocean-Land Model

The model used here consists of coupled general circulation models (GCMs) of the atmosphere and oceans and a simple land model that includes budgets of heat and water. The components of the model interact through the exchange of heat, water and momentum, and are described below. For further details and an evaluation of model performance, see Manabe et al. (1991) and Delworth et al. (2002).

2.1. ATMOSPHERIC AND LAND COMPONENTS

The atmospheric component of the coupled atmosphere-ocean-land climate model solves the equations of motion on a sphere using the spectral transform method (Orsag, 1970). Horizontal distributions of variables are represented by truncated series of spherical harmonics and grid point values, with zonal truncation at wave number 30. The corresponding transform grid has a resolution of 3.75° longitudes by 2.25° latitudes. In the vertical direction, there are 14 unevenly spaced levels for finite difference computation. A seasonally varying insolation is given at the top of the atmosphere. The effects of clouds, water vapor, carbon dioxide and ozone are included in the calculation of solar and terrestrial radiation. Clouds are predicted whenever relative humidity exceeds a critical threshold that varies with height. Precipitation is simulated whenever the predicted water content of air exceeds saturation. The vertical redistribution of temperature and water vapor due to moist convection is represented by a simple scheme called moist convective adjustment (Manabe et al., 1965). For simplicity, the moisture-holding capacity of soil is represented by a 'bucket' at each continental grid box, for which a water budget is computed (Manabe, 1969). Evaporation is a function of both soil moisture and

potential evaporation computed assuming a saturated land surface (Milly, 1992). Whenever the predicted water content of the bucket exceeds 15 cm total depth at any grid point, any excess water is assumed to runoff, is collected over a river basin (Figure 3b), and is transported to the river mouth at the ocean.

2.2. OCEANIC COMPONENT

The oceanic component of the coupled model solves numerically the primitive equations of motion. The grid size for the finite difference computation is 1.75° longitudes by 2.25° latitudes, with 18 unevenly spaced levels in the vertical dimension. The horizontal and vertical mixing of momentum, heat and salt by sub-grid scale eddies is parameterized (Bryan and Lewis, 1979). In addition, the mixing of heat and salt along surfaces of constant density by sub-grid scale eddies is included (Redi, 1982). The coupled model uses a relatively simple thermodynamic model of sea ice, in which sea ice moves with surface ocean currents unless it is thicker than 4 meters and converging.

The initial conditions for a time integration of the coupled model have realistic distributions of surface temperature, surface salinity and sea ice; the atmospheric and oceanic components of the model are nearly in equilibrium with these distributions. When the control integration of the model starts from this initial condition, the model climate rapidly drifts towards its own equilibrium state. To minimize the drift, the fluxes of heat and water at the ocean-atmosphere interface are adjusted by an amount that varies seasonally and geographically, but does not change from one year to the next. Identical adjustments are applied to other experiments conducted here, and are independent of the anomalies of temperature and salinity at the oceanic surface, and so neither damp nor amplify the anomalies.

2.3. NUMERICAL EXPERIMENTS

With the temporal variations of atmospheric CO_2 illustrated in Figure 1a, two time integrations of the coupled model are conducted. One is the standard integration (S), in which atmospheric CO_2 remains unchanged. In the second integration ($4 \times$ C), the CO_2 increases at the rate of 1%/year (compounded) until it reaches four times the standard value at the $\sim$140th year and remains unchanged thereafter. Here, the atmospheric CO_2 may be regarded as the CO_2 equivalent of all greenhouse gases combined. The influence of anthropogenic aerosols is not considered, because it is likely to be relatively less important over century-time scales as the emission control of sulfur dioxide is strengthened.

The climatic response to CO_2 quadrupling is estimated from the differences between $4 \times$ C (years 201–300) and S (years 101–1000). To extract the CO_2-induced change from natural variability, the relevant climatic variables are averaged over the periods of 100 years and 900 years for the $4 \times$ C and S, respectively.

Figure 1b contains the time series of annual mean global surface air temperature from $4 \times$ C and S. By the 140th year of $4 \times$ C, when the atmospheric CO_2

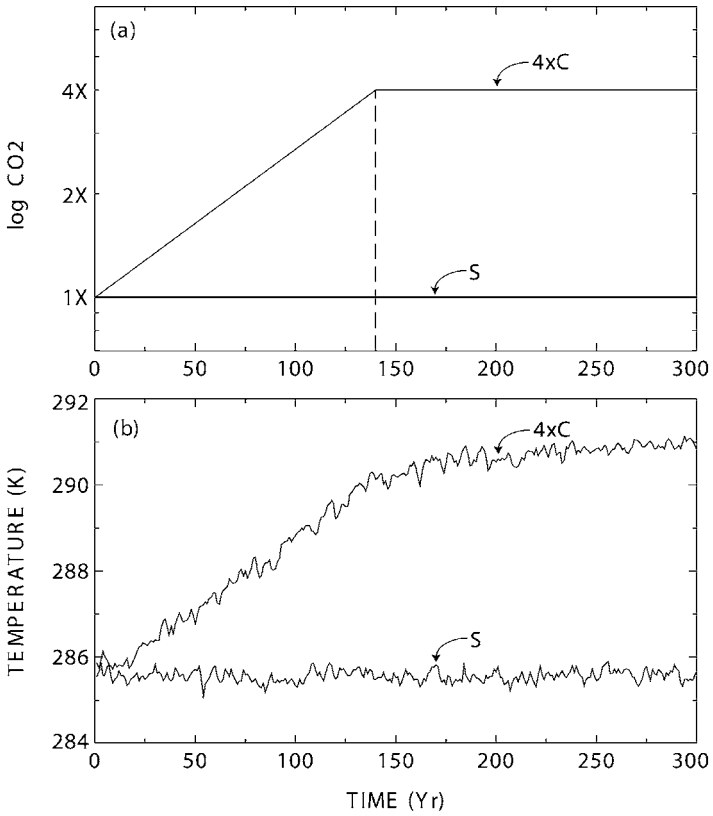

Figure 1. Temporal variation of (a) atmospheric CO_2 concentration (on logarithmic scale), and (b) global mean surface air temperature (°K) from the coupled model.

concentration quadruples, the global surface air temperature increases by ∼5 °C, and it increases very slowly thereafter, yielding a warming of ∼5.5 °C by the year 250. Over continents, the warming is between 5–10 °C and is generally larger than over oceans in middle and high latitudes of the Northern Hemisphere (Figure 2). A notable exception appears over the Arctic Ocean, where warming is as large as 14 °C due to the disappearance of perennial sea ice. On the other hand, warming is small in the Circumpolar Ocean of the Southern Hemisphere due to the upwelling of deep water.

3. River Discharge

In response to the increase in the CO_2 concentration in the atmosphere, temperature increases not only at the Earth's surface but also in the troposphere, thereby inducing an increase in the absolute humidity of air. The changes in temperature and greenhouse gases (e.g., carbon dioxide and water vapor) result in the increase of

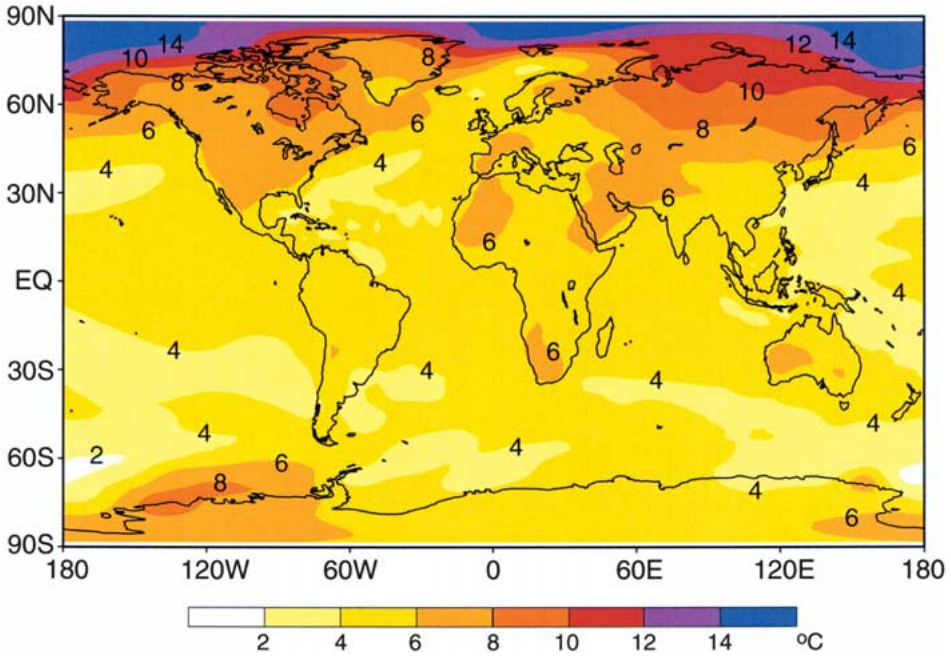

Figure 2. Geographical distribution of the difference in surface air temperature (°C) between 4 × C (years 201–300) and S (years 101–1000).

the net downward flux of infrared radiation, providing more energy to the Earth's surface. Thus, the rate of potential evaporation increases, accelerating evaporation from the surface (e.g., Manabe and Wetherald, 1975; Wetherald and Manabe, 1975). More evaporation, in turn, results in more precipitation. Averaged over the entire globe, both precipitation and evaporation increase by 12.7% in 4 × C (years 201–300). The increase in runoff averaged over all continents turned out to be 14.8%.

Figure 3a illustrates the geographical distribution of the difference in the rate of annual mean runoff between 4 × C and S. Expressed in percentage, the changes are particularly large in high northern latitudes (Table I). For example, the discharge from Arctic rivers such as the Mackenzie and Ob' increases by as much as 40% or more. The large increase is attributable mainly to the increase in absolute humidity of air, which results from the CO_2-induced warming of the troposphere. The increase in absolute humidity, in turn, enhances the northward transport of moisture by cyclonic waves, thereby increasing precipitation and runoff in high latitudes. A large sensitivity of high-latitude runoff to greenhouse forcing is consistent with recent observations (Peterson et al., 2002), although we have not evaluated the detectability of such an early trend.

In low latitudes, the increase in runoff is particularly large in the three regions of intense continental precipitation: Southeast Asia and Indinesia, South America,

and the coastal region of Africa near the Gulf of Guinea (Figure 3a). This is why the discharges from the Ganga-Brahmaputra and Amazonas Rivers increase by as much as 49% and 23%, respectively. When the absolute humidity of air increases accompanying global warming, the supply of moisture to the tropical rainbelt through the trade wind increases and is responsible for the increase in precipitation and runoff over the regions of intense precipitation. The large percentage increase in runoff from the Ganga-Brahmaputra is attributable to not only to the increase in the absolute humidity of air but also to the intensification of the South Asian monsoon circulation. Outside the regions of intense continental precipitation, however, precipitation does not necessarily increase or even decreases, reducing the discharge from some tropical rivers such as the Nile and Mekong. The failure of precipitation to increase in the catchments of these rivers may be attributable to the compensating changes in the vertical transport of air in the tropics. As noted by Gill (1980), the increase in heat released by condensation associated with the intensification of upward velocity in a region of heavy precipitation in the tropics can amplify stationary wave-disturbances that intensify the compensatory vertical motion over other regions of the tropics.

Although the rate of discharge increases markedly from some European rivers, such as the Volga, it changes relatively little for many mid-latitude rivers, such as the Mississippi, Zambezi and Amur. As Figure 3a shows, the local contribution to runoff hardly changes over very extensive areas in middle latitudes. The rate of discharge increases substantially for some mid-latitude rivers, such as the Chang Jiang and Paraná/Uruguay (Table I). However, these rivers collect much of their runoff in regions of heavy rainfall in low latitudes (Figure 3b).

4. Soil Moisture

As Figure 4a shows, the coupled model simulates at least qualitatively the broad scale distribution of continental aridity. For example, the regions of very low soil moisture simulated by the model correspond reasonably well with the major arid regions of the world: the Gobi and Great Indian Deserts of Eurasia, North American Deserts, the Patagonian Desert of South America, and Sahara and Kalahari Deserts of Africa. Regions of relatively low soil moisture simulated by the model also correspond approximately to many semi-arid regions of the world, such as the western plains of North America, the northeastern region of China, the Mediterranean coast of Europe, and the grasslands of Africa, South America, and Australia.

Here we discuss how the soil moisture changes in response to the quadrupling of atmospheric carbon dioxide, using Figures 4b and 5, which illustrate the global distribution of the percentage difference in annual mean value of soil moisture between $4 \times$ C and S and its seasonal variation, respectively. Firstly, the discussion is focused on the soil moisture change in many semi-arid regions of the world, which are located in low and middle latitudes. It is followed by a brief discussion of

Table I

Annual mean rates of simulated discharge (D, 10^3 m^3 s^{-1}) from major rivers of the world obtained from S (years 101–1000) and 4 × C (years 201–300) and their percentage difference, $100 \cdot (D_{4\times C}\text{-}D_S)/D_S$. Discharge is the sum of contributions from all grid boxes in each basin (or combination of basins) outlined in Figure 3b. In arid regions, some of these modeled basins (e.g., Niger, Zambezi) include associated areas of internal drainage. Because of insufficient computational resolution of the model, numerical results should be taken only as indicative of the scale of change. (Analogous results obtained by Milly et al. (2002) for some of the extra-tropical rivers differed numerically from these because they were based on gauged drainage areas, whereas our results pertain to river mouths)

River(s)	Control (S)	4 × C	% Change
a. High latitude			
1. Yukon	12.0	17.7	+47
2. Mackenzie	9.0	12.5	+40
3. Yenisey	15.6	19.4	+24
4. Lena	16.7	20.9	+26
5. Ob’	7.7	11.0	+42
b. Mid-latitude			
6. Rhein/Elbe/Seine	5.2	6.3	+20
7. Volga	6.1	9.7	+59
8. Danube/Dnepr	7.5	8.2	+9
9. Columbia	9.2	13.5	+47
10. St Lawrence/Saguenay	15.2	17.1	+12
11. Mississippi	11.6	10.8	–7
12. Amur	9.2	9.4	+3
13. Huang He	16.7	19.8	+18
14. Chang Jiang	59.2	75.5	+28
15. Zambezi	31.1	31.7	+2
16. Paraná/Uruguay	23.5	36.1	+54
c. Low latitude			
17. Amazonas	308.0	379.0	+23
18. Orinoco	34.3	34.5	+1
19. Ganga/Brahmaputra	60.7	90.3	+49
20. Congo	146.0	145.0	–1
21. Nile	55.1	45.4	–18
22. Mekong	42.2	39.6	–6
23. Niger	58.3	61.6	+6

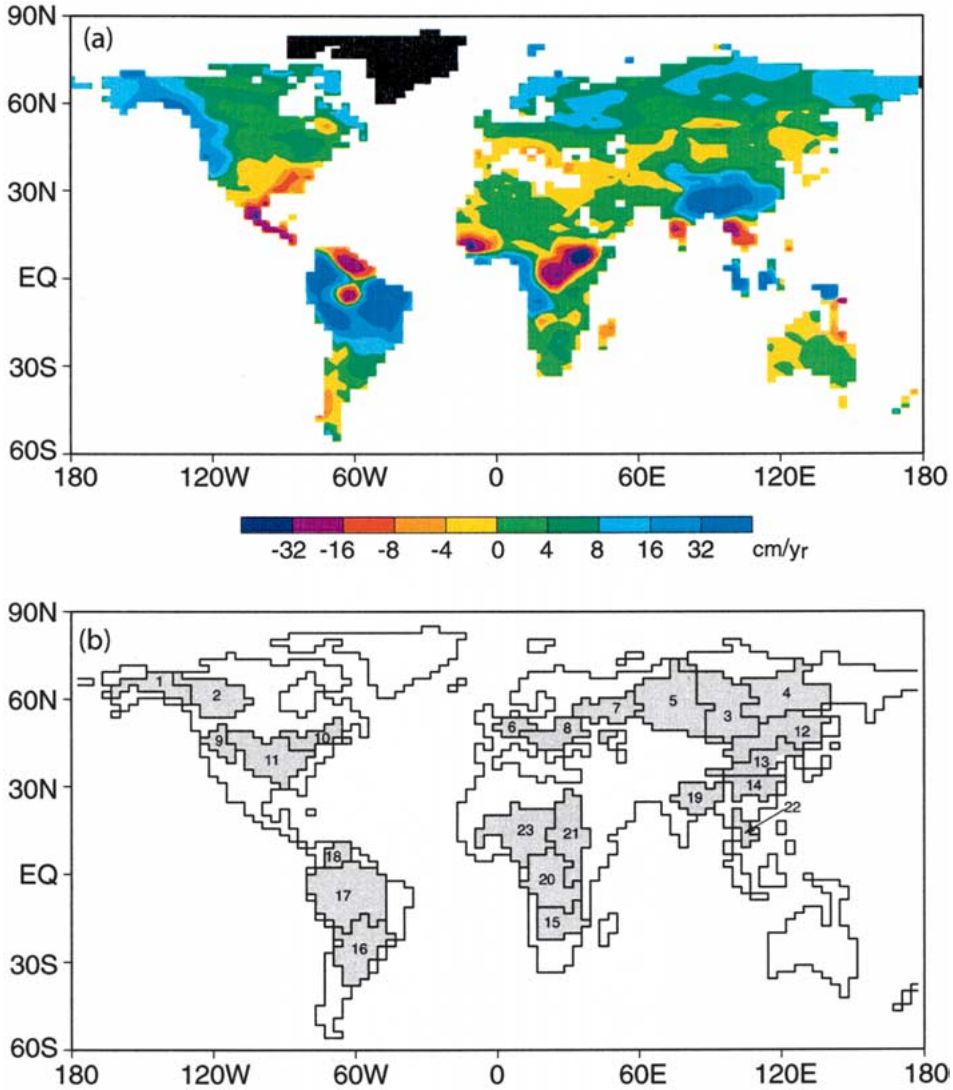

Figure 3. (a) Geographical distribution of the difference in the annual mean rate of runoff (cm/year) between 4 × C (years 201–300) and S (years 101–1000). A 'student-t' test indicates that the difference is statistically significant at 99% or higher confidence level over Siberia, Europe, the northern part of North America, and the Amazonas and Ganga-Brahmaputra River basins, for example. (b) Geographical extents of the basins of major rivers of the world listed in Table I are indicated by shaded regions. The number listed on each basin corresponds to a number in front of the name of each river in Table I. The annual mean rate of the discharge from each river is computed by summing the simulated runoff from all grid boxes in each basin.

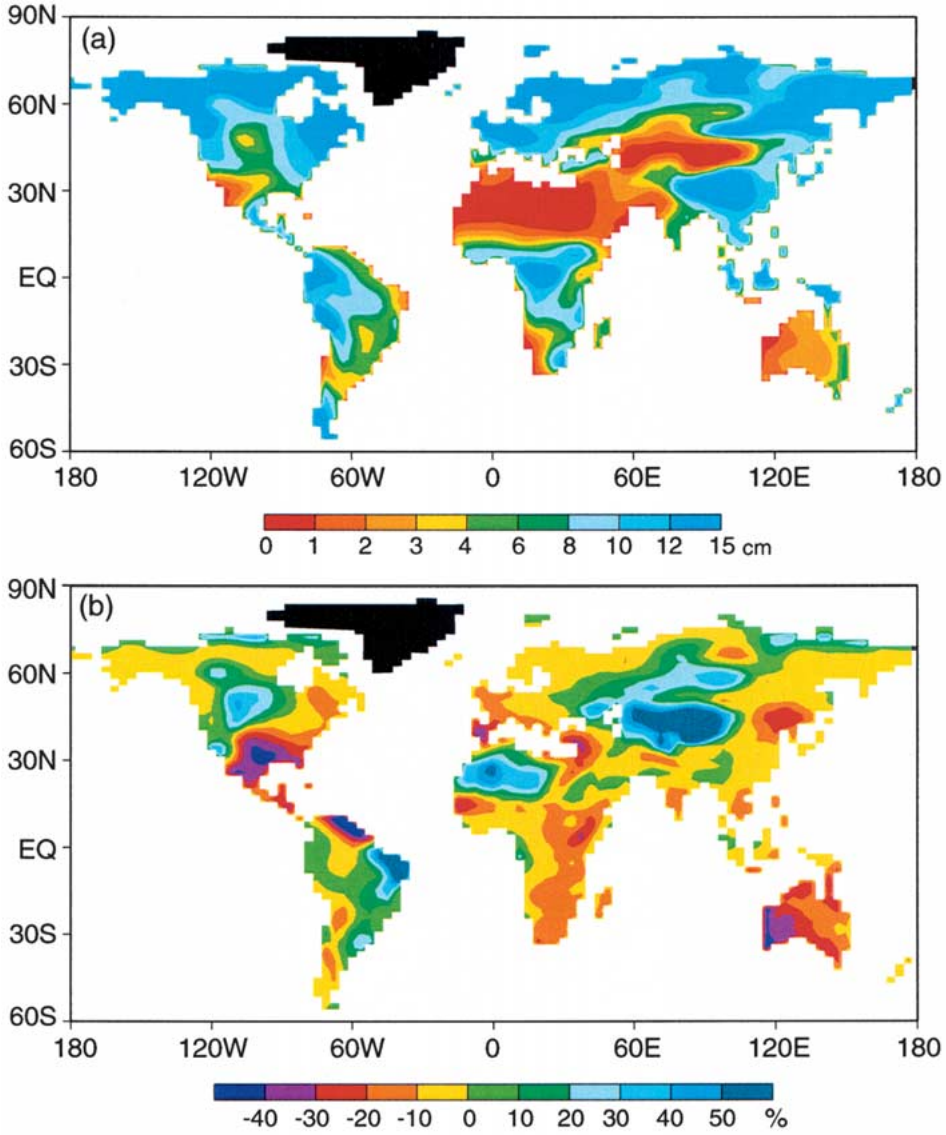

Figure 4. (a) Geographical distribution of annual mean soil moisture (cm) obtained from S. (b) Geographical distribution of the difference (%) in annual mean soil moisture (W) between 4 × C (years 201–300) and S (years 101–1000). The percentage difference is defined as $100 \times (W_{4\times C}\text{-}W_S)/W_S$. A 'student-t' test indicates that the reduction of soil moisture is statistically significant at 99% or higher level over southwestern North America, Mediterranean coast of Europe, the northeastern region of China, and the regions that surround the Australian and Kalahari Deserts, for example.

soil moisture change over very extensive regions of Eurasian and North American Continents in middle and high latitudes.

4.1. SEMI-ARID REGIONS

Figure 4b indicates that annual mean soil moisture decreases in many semi-arid regions of the world, such as southwestern part of North America, Mediterranean coast, the northeastern region of China, the grasslands of Africa and the southern and western coast of Australia. The percentage reduction of soil moisture tends to be large during the relatively dry season (Figure 5). For example, soil moisture is reduced by more than 40% at the Mediterranean coast of Europe in summer (Figure 5a), in the Middle East in summer and fall, in the southwestern part of North America in winter and spring (Figures 5c,d), in South Africa in winter (Figure 5a), and the southern and western coast of Australia in winter and spring (Figures 5a,b).

Figure 4b shows that the region of soil-moisture reduction in the southwestern part of North America extends to the southern part of the U.S.A. (see also Figure 5d). Unfortunately, soil moisture in the control experiment (S) is unrealistically small in the southern part of U.S.A. (Figure 4a), affecting the CO_2-induced soil moisture change there (Figure 4b). If the soil moisture were simulated more realistically in S, the region of soil-moisture reduction would have been limited to the southwestern part of North America, where the actual semi-arid region is located.

It is likely that a reduction of soil moisture in semi-arid regions would induce the outward expansion of major deserts of the world, such as the North American Desert, the Sahara and the Kalahari Deserts of Africa, Patagonian Desert of South America, and the Australian Desert. The reduction of soil moisture in the northeastern region of China could induce the eastward extension of the Gobi Desert.

In a semi-arid region, the amount of soil moisture is essentially determined such that it satisfies the balance between precipitation and evaporation (Milly, 1992). If a percentage increase in precipitation is smaller than that in potential evaporation (defined in the caption of Figure 6), then soil moisture decreases, thereby restoring the balance between precipitation and evaporation. As Figure 6a indicates, the percentage change in annual precipitation is negative over the southern part of North America, Mediterranean Sea and its immediate vicinity, and southern India and Indochina. On the other hand, the percentage change in the annual mean rate of potential evaporation (Figure 6b) increases almost everywhere over continents resulting from the CO_2-induced increase in the downward flux of infrared radiation. The difference between these two percentage changes is illustrated in Figure 6c. This figure shows that the difference is negative, indicating that the percentage change in precipitation is less than that of potential evaporation in many semi-arid regions such as the Mediterranean coast, the northeastern region of China, the southwestern part of North America, Southern India and Indochina and the western

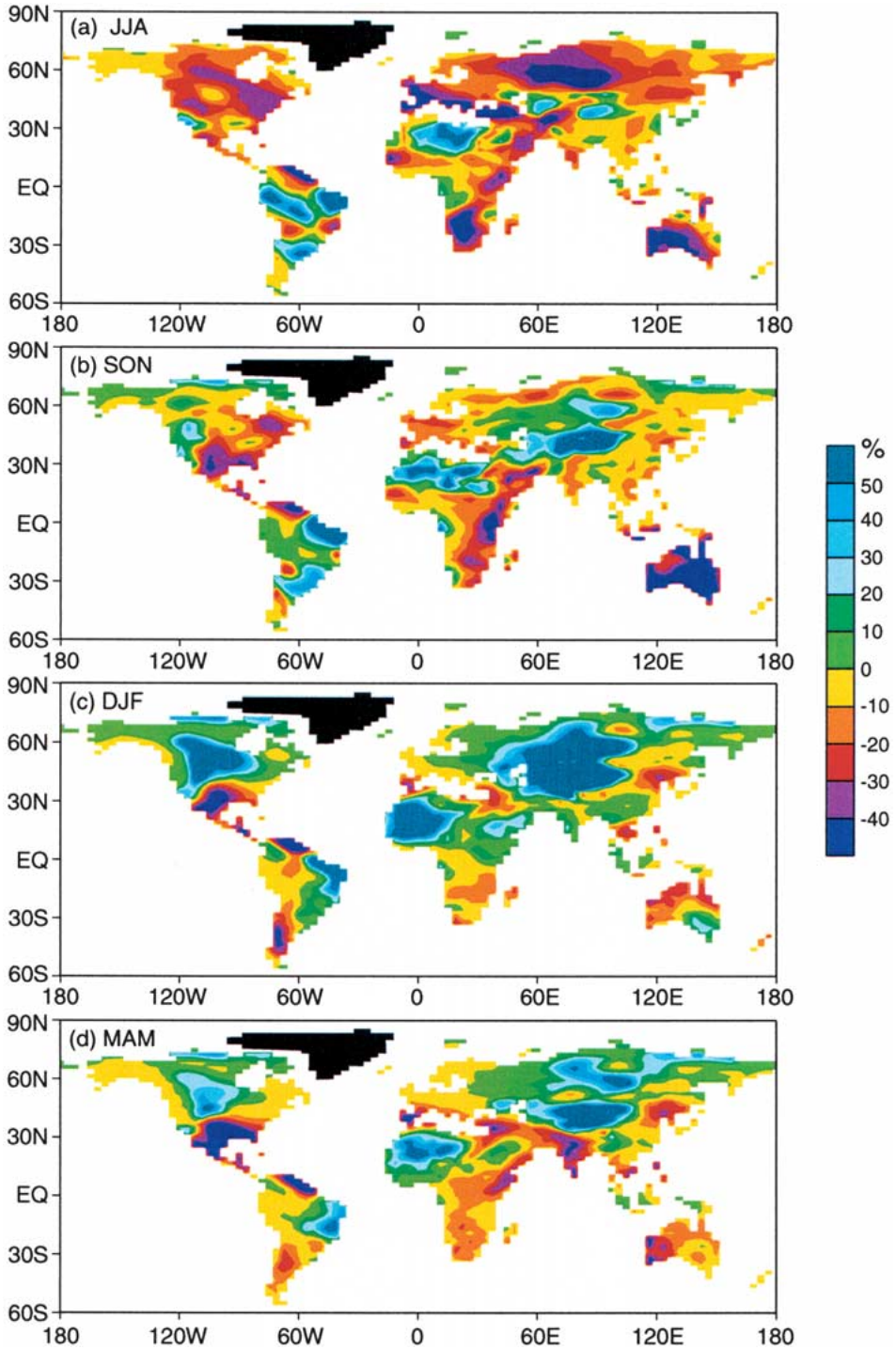

Figure 5. Geographical distribution of the percentage difference in three monthly mean soil moisture (W) between 4 × C (years 201–300) and S (year 101–1000). The percentage difference of W is defined as 100 $(W_{4\times C}\text{-}W_S)/W_S$. (a) June–July–August. (b) September–October–November. (c) December–January–February. (d) March–April–May.

and southern coast of Australia. To maintain the balance between precipitation and evaporation in these regions, it is necessary to keep soil moisture at reduced levels. This is the main reason why the percentage reduction of soil moisture is pronounced in many semi-arid regions of the world as Figure 4b indicates.

In many semi-arid regions of the world, where the increase in temperature is relatively large in the near-surface layer of the atmosphere, relative humidity decreases or fails to increase despite the increase in evaporation from the oceans. This may be one of the important reasons why precipitation decreases in many of these regions. There are other reasons for the reduction of precipitation in some of semi-arid regions. A modeling study conducted by Rodwell and Hoskins (1996) indicates that, in summer, the increase in the heat of condensation over the Indian subcontinents generates the stationary Rossby wave pattern to the west, thereby intensifying the adiabatic descents over and around Mediterranean Sea. One can speculate that an increase in precipitation over a tropical region may generate stationary waves, which intensify the subsidence and reduce precipitation in some of semi-arid regions of the world.

As soil moisture is reduced in a semi-arid region, the relative humidity decreases in the lower troposphere due to the reduction in the ratio of latent to sensible heat flux from the continental surface. The reduction of relative humidity, in turn, results in the reduction of precipitation and the further reduction of soil moisture.

4.2. SUMMER DRYNESS/WINTER WETNESS

Over very extensive regions of the Eurasian and North American continents in middle to high latitudes, soil moisture decreases in summer but increases in winter, in contrast to the situation in semi-arid regions. In summer, the percentage reduction exceeds 30% over certain regions of Siberia and Canada. On the other hand, in winter, soil moisture increases substantially in these regions.

The physical mechanism responsible for the summer-winter reversal in the soil moisture change in middle and high northern latitudes was discussed in details in the preceding studies (e.g., Wetherald and Manabe, 1995, 2002). Therefore, only

Figure 6 (facing page). Geographical distributions of the percentage difference (%) in annual mean rates of precipitation (a) and potential evaporation (b) between 4 × C (years 201–300) and S (years 101–1000). (c) Geographical distribution of (a) minus (b). Here, the potential evaporation is defined as the sum of net downward fluxes of solar and terrestrial radiation at the Earth's surface. It represents the absorption rate of radiative energy by continental surface and is approximately equal to the potential evaporation defined by Budyko (1956), i.e., the radiative energy available for evaporation from hypothetically wet surface. (See Milly (1992) for further discussion of this subject.) The percentage difference of a variable X is defined as 100 $(X_{4\times C}\text{-}X_S)/X_S$.

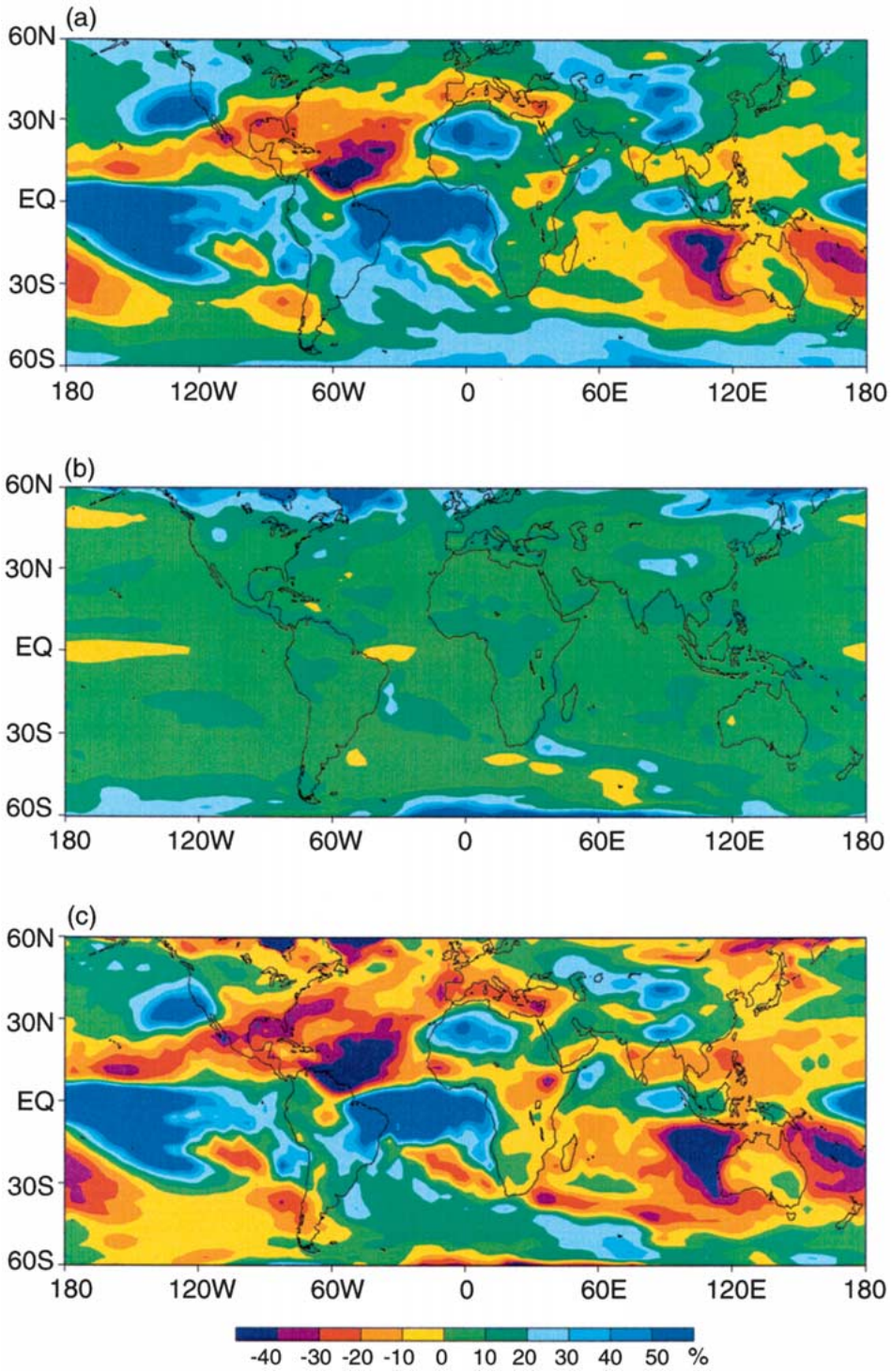
(a)
60N
30N
EQ
30S
60S
180
120W
60W
0
60E
120E
180
(b)
60N
30N
EQ
30S
60S
180
120W
60W
0
60E
120E
180
(c)
60N
30N
EQ
30S
60S
180
120W
60W
0
60E
120E
180
-40 -30 -20 -10 0 10 20 30 40 50 %

Figure 6.

a brief discussion is presented here. In contrast to the situation over oceans, continental surface temperature in middle and high latitudes undergoes a large seasonal variation. In winter, when surface temperature is very low in these latitudes, the increase in the downward flux of radiation due to the increase of atmospheric greenhouse gases contributes mainly to the increase of sensible heat flux rather than that of latent heat flux of evaporation. This is why the rate of evaporation hardly increases accompanying global warming in winter. On the other hand, precipitation increases over continents due to the increase in the supply of water vapor from the oceans, where the annual variation of surface temperature is small and evaporation increases throughout a year. Since temperature is very low over continents during winter, saturation vapor pressure of air hardly increases despite the increase in temperature. Thus, relative humidity tends to increase in the lower troposphere, inducing the slight increase in precipitation. The increase in precipitation, in turn, results in the slight increase in soil moisture as described above.

In summer, when surface temperature and its saturation vapor pressure are high over continents, a major fraction of the heating due to the increase in greenhouse gases is used to enhance evaporation. On the other hand, precipitation fails to increase by a similar percentage, or even decreases over Siberia and Canada, where relative humidity decreases in the near-surface layer of the atmosphere resulting from the relatively large increase in temperature. This is why soil moisture is reduced in summer over very extensive regions from the middle to high latitudes of the Northern Hemisphere. The timing of snowmelt in spring is another important factor responsible for the summer reduction of soil moisture. As surface temperature increases accompanying global warming, the snowmelt season ends earlier and exposes the soil surface to intense solar radiation. Thus, the spring-to-summer reduction of soil moisture begins earlier, thereby contributing to the reduction of soil moisture in summer. In due course, the reduction of soil moisture results in the reduction of evaporation, which reduces the relative humidity in the lower troposphere. The decrease in relative humidity, in turn, reduces rainfall, thereby drying soil further in the late summer.

In contrast to the situation discussed above, simulated annual mean precipitation and soil moisture increase very slightly (but in substantial percentage) in summer as well as in winter over some very arid regions such as Sahara, and Central Asia (Figures 5 and 6). Although we have not analyzed the specific mechanism responsible for the increase in precipitation in summer, a large increase in surface temperature may be responsible for enhancing very sporadic moist convective activity, thereby increasing precipitation and soil moisture over very arid regions. More detailed analysis of simulated precipitation is needed to determine the reason why simulated precipitation increases slightly even in summer in very arid regions of the world.

5. Discussion

In a preceding study, Wetherald and Manabe (2002) estimated the future changes in water availability expected by the middle of the 21st century, conducting a multi-member ensemble of numerical experiments. The geographical distributions of the changes obtained from the study (see Figures 5a, 11a, and 10 of their paper) were similar to those obtained in the present study, which are much larger. The consistency between the two studies implies that the changes reported here are mainly CO_2-induced, with a much smaller contribution from unforced natural variability.

The similarity between the results from the two studies is attributable in no small part to the long-term averaging applied to the relevant hydrologic variables such as precipitation, soil moisture, and river discharge. In the preceding study, a hydrologic variable around the middle of the 21st century was estimated from the eight thirty year averages over the period between 2035 and 2065. The length of the time averaging period involved is 240 ($= 30 \times 8$) years. In the present study, which involves a larger CO_2-change, hydrologic variables are averaged over the period of 100 years between the 200th and 300th year of the $4 \times$ C. The CO_2-induced changes are then estimated from the difference between the time mean values thus obtained and the 900 year average from the control experiment. Through the very long time-averaging, it is possible to reduce sufficiently the sampling noise due to unforced, large natural variability and extract the CO_2-induced changes of hydrologic variables, which are consistent between the two studies.

One of the critical factors that determine the water availability at the continental surface is the change in annual mean precipitation. With the notable exception of Indochina and Southern India, the geographical patterns of simulated, multi-member ensemble mean changes in annual precipitation obtained from the preceding study (see Figure 12 of Wetherald and Manabe (2002), in which the unit of precipitation change should have been mm/day rather than cm/day) are similar to that of the multi-model ensemble mean change recently obtained by IPCC for the scenario IS92a (see Figure 9.11c in Cubasch et al. (2001)). For example, the multi-model precipitation from IPCC increases significantly over Siberia and Canada, and decreases over the southwestern part of North America, the western and southern coasts of Australia, Mediterranean Sea and its immediate vicinity, and South Africa in qualitative agreement with the results from our preceding as well as present studies. The qualitative similarity between the patterns of precipitation changes obtained from the three studies suggests that the underlying physical mechanisms are similar. One should note, however, that there is a large quantitative difference among global mean precipitation changes obtained by various models submitted to IPCC (Allen and Ingram, 2002). Given the IS92a scenario, the global mean change in precipitation from the present model belongs to the upper half of the changes compiled by Cubasch et al. (2001).

As described in Section 2, the land surface component of the coupled model used here is highly idealized. It does not seem likely, however, that the large-scale

pattern of the change in water availability would be altered substantially, had we used a more detailed land surface scheme. For example, in many semi-arid regions of the world, soil moisture is essentially determined such that it satisfies the balance between precipitation and evaporation (Milly, 1992). Thus, the reduction of soil moisture in semi-arid regions results from the difference between the changes in potential evaporation and precipitation, and is not very sensitive to the details of land surface parameterization. The experiment conducted here also indicates the marked increase in discharge from high latitude rivers and a few major tropical rivers. Our analysis reveals that it is attributable to the increase of precipitation, which is much larger than that of evaporation. Again, it does not seem likely that the result would be very different had we used a more detailed parameterization.

On the other hand, the summer reduction of soil moisture in middle to high latitudes might not be as pronounced, had we used a land surface scheme that incorporates the moisture-holding capacity of the deeper soil layer that retains moisture from wetter winter. In very high latitudes, where the surface is covered by permafrost, one should not take too seriously the simulated change of soil moisture since the land surface scheme used here does not incorporate the freezing and melting of water in soil. One should also note that the model used here does not include various biospheric feedbacks. For example, the spread of deserts discussed above could lead to a change in albedo of the continental surface. The change in the water balance of soil could also induce a response by plant root systems, leading to changes in effective water-holding capacity of soil (Milly, 1997). Therefore, it is very desirable to reevaluate the results obtained here, using a model with biospheric feedback processes.

The computational resolution of the coupled model used here is not sufficient to resolve the atmospheric circulation over and around major mountain ranges such as Tibetan Plateau, European Alps, and Rocky and Andes mountain ranges. Thus, the model fails to simulate satisfactorily the near- and far-field effect of these mountains upon the global distribution of precipitation. In order to obtain a reliable estimate of the future change in water availability, it is therefore necessary to conduct a similar numerical experiment using a coupled model with much higher resolution.

6. Concluding Remarks

If the atmospheric concentration of carbon dioxide continues to increase, the reduction of soil moisture in many semi-arid regions of the world may become increasingly noticeable during the 21st century. By the latter half of the 22nd century, when CO_2 concentration may quadruple, the soil moisture change could become very substantial and almost as large as the change described in this study. To make the matter worse, the increase in surface temperature in these regions would accelerate evaporation from irrigated croplands, greatly increasing the de-

mand for water. Unfortunately, runoff from these semi-arid regions is not likely to increase significantly or may even decrease slightly as global warming proceeds. It is therefore likely that the shortage of water in these regions will become very acute during the next few centuries. On the other hand, an increasingly excessive amount of water is likely to be available in water-rich regions in high northern latitudes. The implied amplification of existing differences in water availability between different regions could present a profound challenge to the water managers of the world.

Acknowledgements

K. A. Dunne constructed the drainage basins that were incorporated into the coupled model. A. J. Broccoli, K. L. Findell, and H. Lins provided very helpful reviews.

References

Allen, M. R. and Ingram, W. J.: 2002, 'Constraints on Future Changes in Climate and the Hydrologic Cycle', *Nature* **419**, 224–232.

Bryan K. and Lewis L. J.: 1979, 'A Water Mass Model of the World Oceans', *J. Geophys. Res.* **84**, 2503–2517.

Budyko, M. I.: 1956, *Heat Balance of Earth's Surface* (in Russan), Gidrometeoizdat, 255 pp.

Cubasch et al.: 2001, 'Projection of Future Climate Change', Chapter 9 in *Climate Change 2001: The Scientific Basis*, Cambridge University Press, Cambridge, pp. 524–582.

Delworth, T. L., Stouffer, R. J. Dixon, K. W., Spelman, M. J., Knutson, T. R., Broccoli, A. J., Kushner, P. J., and Wetherald, R. T.: 2002, 'Review of Simulations of Climate Variability and Change with the GFDL R30 Coupled Climate Model', *Clim. Dyn.* **19**, 555–574.

Gill, A. E.: 1980, 'Some Simple Solutions for Heat-Induced Tropical Circulation', *Quart. J. Roy. Meteorol. Soc.* **106**, 447–462.

IPCC: 1992, 'Climate Change, 1992: The Supplimentary Report to the IPCC Scientific Assessment', in Houghton, J. T., Callander, B. A., and Varney, S. K. (eds.), Cambridge University Press, Cambridge, U.K., 269 pp.

Manabe, S.: 1969, 'Climate and Ocean Circulation: 1, The Atmospheric Circulation and Hydrology of the Earth's Surface', *Mon. Wea. Rev.* **97**, 739–774.

Manabe, S., Bryan, K., Spelman, M. J., and Bryan, K.: 1991, 'Transient Response of a Coupled Ocean-Atmosphere Model to Gradual Change of Atmospheric CO_2', *J. Climate* **4**, 785–818.

Manabe, S., Smagorinsky, J., and Strickler, R. F.: 1965, 'Simulated Climatology of a General Circulation Model with a Hydrologic Cycle', *Mon. Wea. Rev.* **93**, 769–798.

Manabe, S. and Stouffer, R. J.: 1993, 'Century-Scale Effects of Increased Atmospheric CO_2 on the Ocean-Atmosphere System', *Nature* **364**, 215–218.

Manabe, S. and Stouffer, R. J.: 1994, 'Multi-Century Response of a Coupled Ocean-Atmosphere Model to an Increase of Atmospheric Carbon Dioxide', *J. Climate* **7**, 5–23.

Manabe, S. and Wetherald, R. T.: 1975, 'The Effect of Doubling the CO_2 Concentration on the Climate of a General Circulation Model', *J. Atmos. Sci.* **32**, 3–15.

Milly, P. C. D.: 1992, 'Potential Evaporation and Soil Moisture in General Circulation Models', *J. Climate* **5**, 209–226.

Milly, P. C. D.: 1997, 'Sensitivity of Greenhouse Summer Dryness to Changes in Plant Rooting Characteristics', *Geophys. Res. Lett.* **24**, 269–271.

Milly, P. C. D., Wetherald, R. T., Dunne, K. A., and Delworth, T. L.: 2002, 'Increasing Risk of Great Floods in a Changing Climate', *Nature* **415**, 514–517.

Orsag, S. A.: 1970, 'Transform Method for Calculating Vector-Coupled Sums: Application to the Spectral Form of the Vorticity Equation', *J. Atmos. Sci.* **27**, 890–895.

Peterson, B. J., Holmes, R. M., McClelland, J. W., Vörösmarty, C. J., Lammers, R. B., Shiklomanov, A. I., Shiklomanov, Igor A., and Rahmstorf, S.: 2002, 'Increasing River Discharge to the Arctic Ocean', *Science* **298**, 2171–2173.

Redi M. H.: 1982, 'Oceanic Isopycnal Mixing by Coordinate Rotation', *J. Phys. Oceanog.* **12**, 1154–1158.

Rodwell, M. J. and Hoskins, B. J.: 1996, 'Monsoon and the Dynamics of Deserts', *Quart. J. Roy. Meteorol. Soc.* **122**, 1385–1404.

Walker, J. C. G. and Kasting, J. F.: 1992, 'Effect of Fuel and Forest Conservation on Future Levels of Atmospheric Carbon Dioxide', *Paleogeogr. Paleoclimatol. Paleoecol.* **97**, 151–189.

Wetherald, R. T. and Manabe, S.: 1975, 'The Effect of Changing Solar Constant on the Climate of a General Circulation Model', *J. Atmos. Sci.* **32**, 2044–2059.

Wetherald, R. T. and Manabe, S.: 1995, 'The Mechanism of Summer Dryness Induced by Greenhouse Warming', *J. Climate* **8**, 3096–3108.

Wetherald, R. T. and Manabe, S.: 2002, 'Simulation of Hydrologic Changes Associated with Global Warming', *J. Geophys. Res.* **107**, 4379–4394.

(Received 25 February 2003; in revised form 23 July 2003)